Preprint: DOI: 10.1007/s10596-008-9121-y
To appear in Computational Geosciences, 2009.
The original publication is available at www.springerlink.com

A DISCRETIZATION AND MULTIGRID SOLVER FOR A DARCY-STOKES SYSTEM OF THREE DIMENSIONAL VUGGY POROUS MEDIA*

TODD ARBOGAST† AND MARIO SAN MARTIN GOMEZ†

Abstract. We develop a finite element discretization and multigrid solver for a Darcy-Stokes system of three dimensional *vuggy* porous media, i.e., porous media with cavities. The finite element method uses low order mixed finite elements in the Darcy and Stokes domains, and special transition elements near the Darcy-Stokes interface to allow for tangential discontinuities implied by the Beavers-Joseph boundary condition. We design a multigrid method to solve the resulting saddle point linear system. The intertwining of the Darcy and Stokes subdomains makes the resulting matrix highly ill-conditioned. The velocity field is very irregular, and its discontinuous tangential component at the Darcy-Stokes interface makes it difficult to define intergrid transfer operators. Our definition is based on mass conservation and the analysis of the orders of magnitude of the solution. The coarser grid equations are defined using the Galerkin method. A new smoother of Uzawa type is developed based on taking an optimal step in a good search direction. Our algorithm has a measured convergence factor independent of the size of the system, at least when there are no disconnected vugs. We study the macroscopic effective permeability of a vuggy medium, showing that the influence of vug orientation, shape, and, most importantly, interconnectivity determine the macroscopic flow properties of the medium.

Key words. Darcy-Stokes, vuggy porous medium, Beavers-Joseph boundary condition, mixed finite element, error estimates, multigrid, Uzawa smoother

1. Introduction. We consider the computational simulation of a fluid within a *vuggy* porous medium Ω. This is a porous medium with large void inclusions or cavities (also called *vugs*). We envision these vugs to be spread throughout the rock, so they have a major effect on the flow and transport properties of the medium.

The fluid in the porous matrix, $\Omega_d \subset \Omega$, obeys the Darcy law for the velocity $\mathbf{u}_d = \mathbf{u}|_{\Omega_d}$ and the pressure $p_d = p|_{\Omega_d}$, which is

$$-\mu K^{-1}\mathbf{u}_d + \nabla p_d = g \quad \text{in } \Omega_d, \tag{1.1}$$

where μ is the fluid viscosity, K is the permeability of the porous medium, and g is a force term such as gravity. The free fluid in the vuggy inclusions, $\Omega_s = \Omega \setminus \bar{\Omega}_d$, obeys the Stokes equations. That is, combined with conservation on Ω, and with $(\mathbf{u}_s, p_s) = (\mathbf{u}, p)|_{\Omega_s}$,

$$-2\mu\nabla \cdot D\mathbf{u}_s + \nabla p_s = g \quad \text{in } \Omega_s, \tag{1.2}$$

$$\nabla \cdot \mathbf{u} = f \quad \text{in } \Omega, \tag{1.3}$$

where D denotes the symmetric gradient, i.e., $D\mathbf{v}$ is the matrix such that $(D\mathbf{v})_{ij} = \frac{1}{2}\left(\frac{\partial \mathbf{v}_i}{\partial x_j} + \frac{\partial \mathbf{v}_j}{\partial x_i}\right)$, and f is an external source or sink (i.e., the effects of wells). On the

*This work was supported by the U.S. National Science Foundation under grants DMS-0074310 and DMS-0417431.

†The University of Texas at Austin; Department of Mathematics; 1 University Station C1200; Austin, TX 78712; and The University of Texas at Austin; Institute for Computational Engineering and Sciences; 1 University Station C0200; Austin, TX 78712 (arbogast@ices.utexas.edu, mario@ices.utexas.edu).

interface $\Gamma = \bar{\Omega}_s \cap \bar{\Omega}_d$ between the two regions, the fluid obeys the principle of mass flux continuity, continuity of normal stress, and the special Beavers-Joseph-Saffmann boundary condition on the tangential stress [6, 25, 19], which are

$$\mathbf{u}_s \cdot \nu = \mathbf{u}_d \cdot \nu \qquad \text{on } \Gamma, \tag{1.4}$$

$$2\mu\nu \cdot D\mathbf{u}_s \cdot \nu = p_s - p_d \qquad \text{on } \Gamma, \tag{1.5}$$

$$2\nu \cdot D\mathbf{u}_s \cdot \tau_k = -\alpha K^{-1/2} \mathbf{u}_s \cdot \tau_k \quad \text{on } \Gamma,\ k = 1, 2, \tag{1.6}$$

where α is the Beavers-Joseph-Saffman constant, τ_1 and τ_2 denote two orthogonal unit tangent vectors to the interface Γ, and ν is the outer unit normal vector to $\partial\Omega_s$ (and later to $\partial\Omega$). Note that (1.6) allows for a discontinuity in the tangential velocity. Finally, on the outer boundary,

$$\mathbf{u} \cdot \nu = u_N \quad \text{on } \Gamma_N \subset \partial\Omega, \tag{1.7}$$

$$p = p_D \quad \text{on } \Gamma_{D,d} = \partial\Omega \cap \partial\Omega_d \setminus \bar{\Gamma}_N, \tag{1.8}$$

$$p - 2\mu\nu \cdot D\mathbf{u} \cdot \nu = p_D \quad \text{on } \Gamma_{D,s} = \partial\Omega \cap \partial\Omega_s \setminus \bar{\Gamma}_N, \tag{1.9}$$

$$\mathbf{u} \cdot \tau_k = 0 \qquad \text{on } \partial\Omega \cap \partial\Omega_s,\ k = 1, 2, \tag{1.10}$$

where u_N and p_D are given. Let $\Gamma_D = \Gamma_{D,d} \cup \Gamma_{D,s} = \partial\Omega \setminus \bar{\Gamma}_N$.

Numerical techniques have been developed for the treatment of Darcy-Stokes systems, using different finite elements in the two regions (see, e.g., [26, 17, 14, 20, 13, 22, 16, 12]). In Arbogast and Brunson [2], a single set of element basis functions apply equally well to the Darcy and Stokes regions, and so apply naturally to the case when the two subdomains are intertwined, as occurs in a vuggy medium. Specially modified transition elements are used to account for discontinuities in the tangential velocity of the solution. These finite elements were defined for two dimensional domains; we extend them to three dimensions in this paper, and so define a finite element method for approximating the solution to our problem (1.1)–(1.10).

By restricting to the basis finite elements, these discrete equations result in a symmetric system of linear equations of *saddle-point* form

$$\begin{bmatrix} A & B \\ B^t & 0 \end{bmatrix} \begin{bmatrix} u \\ p \end{bmatrix} = \begin{bmatrix} g \\ f \end{bmatrix}, \tag{1.11}$$

abusing the notation a bit in that the symbols g, f, and p are used in two different ways, although no confusion should arise. Because the flow is described by different equations in the vugs and in the porous matrix, and both subdomains are intertwined, the resulting matrix is highly oscillating and hence, ill-conditioned.

In [2], an inexact Uzawa algorithm was used to solve (1.11), but it required a good preconditioner to converge at a reasonable rate. The authors noted that on a 2-D rectangular grid, the x and y components of the solution partition A as $A = \begin{bmatrix} A_{xx} & A_{xy} \\ A_{yx} & A_{yy} \end{bmatrix}$, and so they took $A^{-1} \approx \begin{bmatrix} A_{xx}^{-1} & 0 \\ 0 & A_{yy}^{-1} \end{bmatrix}$. This preconditioner turned out to be very effective, but quite expensive to compute, since it still required factoring two matrices of half size. The use of a simpler preconditioner considerably reduced the rate of convergence to intolerable levels.

In this paper, we design a multigrid solver for (1.11). It is well known that a system with highly oscillating coefficients poses serious challenges, since the lack of regularity of the solution makes it difficult to define multigrid prolongation and restriction operators.

Operator-dependent interpolation has been proposed for the diffusion equation ($\Omega_d = \Omega$, and no Stokes region appears) with a jumping coefficient K [1, 28]. In these works, the irregularity of $-K/\mu$ implies a discontinuity of the gradient of the solution p, but the product of these two terms, the velocity flux $\mathbf{u}$, should be continuous. The prolongation operator is designed to preserve the continuity of this flux. Still, from one point to another in the domain, the equation changes only because the coefficient changes. Our case is more complicated, because the differential operator itself changes dramatically depending on the subdomain Ω_s or Ω_d, and for vuggy systems, these two subdomains intertwine in complex ways.

Another tool used to deal with varying coefficients is algebraic multigrid [24, 27], in which geometric grids are not considered at all. The starting point is a linear system and all the arguments come from the analysis of the structure of the matrix. We did not follow this approach because of the physical nature of our problem. As explained below, our definition of the prolongation operator is based on an interpretation of coarse grid quantities as average fluxes on coarse grid edges, the use of mass conservation, and the analysis of the relative orders of magnitude of the fluxes in the Darcy and Stokes subdomains.

The choice of multigrid smoother is also quite important. Standard Uzawa smoothing is not very robust. We develop a new Uzawa smoother that works well for our problem. It is based on taking an optimal step in a good search direction. We prove that the coarse grid equations at all levels are well posed and show numerically that our algorithm has a measured convergence factor independent of the size of the system, at least when there are no disconnected vugs. Our method is also suitable for parallelization, which we plan to do in the future.

We then use our solver to investigate by simulations the macroscopic flow properties of vuggy porous media. Flow properties had been previously studied in the two dimensional case in [3, 11]. We confirm and extend these computational results in three dimensions by considering straight vug channels, constricted vug channels, meandering vug channels, and disconnected vugs. Our three dimensional numerical studies show that the orientation, shape, and, most importantly, the interconnectivity of the vugs determine the macroscopic effective permeability of the medium.

A brief outline of the paper follows. In §2, we present our finite element method for three dimensional domains. In §3, we present our multigrid solver for the discretized system. Most importantly, we define our prolongation operators motivated by physical principles, present our new Uzawa smoother, and verify that our procedure is well defined. In §4, we present some numerical tests of the multigrid solver, showing that it works well in practice. Finally, in §5, we present our study of effective permeabilities of vuggy media.

2. Discretization of the differential system. We rewrite the system as a variational problem (for more details, the interested reader may consult, e.g., [20, 4, 2]). First some notation. Let $L^2(\omega) = \{f : \int_\omega |f(x)|^2\, dx < \infty\}$ denote the usual Lebesgue space of square integrable functions on the domain ω, let $H^k(\omega)$ denote the Sobolev space of functions in $L^2(\omega)$ with distributional derivatives up to order k in $L^2(\omega)$, and denote the usual Hilbert space of vector-valued functions $H(\mathrm{div}, \omega) = \{\mathbf{v} \in (L^2(\omega))^3 : \nabla \cdot \mathbf{v} \in L^2(\omega)\}$. We need the function spaces

$$\begin{aligned}\mathbf{V}_\psi = \{&\mathbf{v} \in H(\mathrm{div}, \Omega) : \mathbf{v}_s = \mathbf{v}|_{\Omega_s} \in (H^1(\Omega_s))^3,\ \mathbf{v} \cdot \nu = \psi \text{ on } \Gamma_N,\\ &\text{and } \mathbf{v} \cdot \tau_k = 0 \text{ on } \partial\Omega_s \cap \partial\Omega,\ k = 1, 2\},\\ W = L^2(\Omega) \quad &(W = L^2(\Omega)/\mathbb{R} \text{ if } \Gamma_N = \partial\Omega).\end{aligned}$$

We let $(\cdot,\cdot)_\omega$ denote various $L^2(\omega)$ inner products, depending on the arguments. For scalar functions, $(\psi_1,\psi_2)_\omega = \int_\omega \psi_1(x)\,\psi_2(x)\,dx$. When these are vectors, we have $(\psi_1,\psi_2)_\omega = (\psi_1\cdot\psi_2,1)_\omega = \sum_i(\psi_{1,i},\psi_{2,i})_\omega$, and when these are matrices, we have $(\psi_1,\psi_2)_\omega = (\psi_1:\psi_2,1)_\omega = \sum_{i,j}(\psi_{1,ij},\psi_{2,ij})_\omega$.

The variational formulation of the boundary value problem (1.1)–(1.10) is to find velocity $\mathbf{u}\in\mathbf{V}_{u_N}$ and pressure $p\in W$, such that, for all $\mathbf{v}\in\mathbf{V}_0$ and $w\in W$,

$$\begin{aligned} 2\mu(D\mathbf{u},D\mathbf{v})_{\Omega_s} + \sum_{k=1}^{2}\mu(\alpha K^{-1/2}\mathbf{u}_s\cdot\tau_k,\mathbf{v}_s\cdot\tau_k)_\Gamma \\ + \mu(K^{-1}\mathbf{u},\mathbf{v})_{\Omega_d} - (p,\nabla\cdot\mathbf{v})_\Omega = (g,\mathbf{v})_\Omega - (p_D,\mathbf{v}\cdot\nu)_{\Gamma_D}, \end{aligned} \tag{2.1}$$

$$(\nabla\cdot\mathbf{u},w)_\Omega = (f,w)_\Omega. \tag{2.2}$$

2.1. The three dimensional finite elements. Discretization of (2.1)–(2.2) is achieved using a standard Stokes finite element space [5, 15], modified to allow discontinuities of the tangential component of the velocity along the Darcy-Stokes interface. To do this, we must assume that both Ω_s and Ω_d are unions of rectangles, so Γ does not cut any element. We define our elements in three dimensions, which are a generalization of the elements presented in [2] for two dimensional domains.

Let $E=(-a,a)\times(-b,b)\times(-c,c)$ be a reference rectangular element in $\mathbb{R}^3$. On this element, the pressure is approximated by a constant.

To define the velocity approximation, we concentrate on x-velocity components, the other components being analogous. Let $Q_{i,j,k}(E)$ be the space of polynomials defined on E of degree i in x, j in y, and k in z. Let $B_x^\pm$ be the "bubble" polynomials on E of the form

$$B_x^\pm(x,y,z) = \frac{9}{8ab^2c^2}(x\pm a)(y^2-b^2)(z^2-c^2).$$

On each unmodified element, the x-velocity is approximated in the space

$$V_{E,s}^x = Q_{1,1,1}(E) + \operatorname{span}\{B_x^-,\ B_x^+\},$$

i.e., trilinears augmented with the span of the two bubble functions.

The choice of finite element basis is critical to the sequel. We have 10 degrees of freedom for each Cartesian direction. We choose the value at each of the 8 corners of the three dimensional rectangle as a degree of freedom,

$$v(\pm a,\pm b,\pm c).$$

We also choose the average flux per unit area through the faces perpendicular to the given Cartesian direction, i.e.,

$$\frac{1}{4bc}\int_{-b}^{b}\int_{-c}^{c} v(\pm a,y,z)\,dz\,dy.$$

The nodal basis includes $B_x^\pm$, since

$$B_x^+(\pm a,\pm b,\pm c)=0 \quad\text{and}\quad \frac{1}{4bc}\int_{-b}^{b}\int_{-c}^{c} B_x^+(x,y,z)\,dz\,dy = \begin{cases} 0 & \text{if } x=-a,\\ 1 & \text{if } x=a;\end{cases}$$

that is, B_x^+ is the function whose average flux per unit area through the face $x=a$ is 1, and the rest of its degrees of freedom are equal to 0 (i.e., its corner values and

average flux through face $x = -a$). The function B_x^- is similar, but the roles of the two faces are interchanged. The rest of the nodal basis is given by

$$v_{\pm a,\pm b,\pm c}(x,y,z) = \frac{1}{8abc}(x \pm a)(y \pm b)(z \pm c) - \frac{9}{32ab^2c^2}(x \pm a)(y^2 - a^2)(z^2 - b^2),$$

which are the functions in $V_{E,s}^x$ with all degrees of freedom equal to 0 except for the value at corner $(\pm a, \pm b, \pm c)$, which is 1. In terms of the 10 nodal basis functions, then, the unmodified space is

$$V_{E,s}^x = \text{span}\{v_{-a,-b,-c},\ v_{a,-b,-c},\ v_{-a,b,-c},\ v_{a,b,-c},\\ v_{-a,-b,c},\ v_{a,-b,c},\ v_{-a,b,c},\ v_{a,b,c},\ B_x^-,\ B_x^+\}.$$

This element was defined and analyzed in [5] for Darcy flow.

The standard elements need to be modified near the Darcy-Stokes interface Γ to allow for tangential discontinuities in the velocity. We accomplish this be removing corner degrees of freedom. However, we do not merely remove basis functions; rather, we must reduce the dimension of the polynomial space. Moreover, to reduce the size of the overall system as much as possible, we remove all unnecessary corner degrees of freedom in the Darcy domain.

If E is a Stokes element, i.e., $E \subset \Omega_s$, then we need to apply the symmetric gradient to $\mathbf{u}$ and $\mathbf{v}$, so we need to approximate by a continuous finite element. Therefore we keep all corner degrees of freedom in the Stokes elements. However, if E is a Darcy element, i.e., $E \subset \Omega_d$, we do not necessarily need the corner degrees of freedom. In fact, we only need them when fluid flows from a Darcy region into a Stokes region (i.e., normal to Γ).

For Darcy elements strictly away from Γ, we use elements without corner degrees of freedom. These are the standard lowest order Raviart-Thomas finite elements [21, 10, 23]. The x-component basis functions are

$$R_x^{\pm}(x,y,z) = \frac{1}{8abc}(x \pm a),$$

which are functions whose average flux per unit area through face $x = \pm a$ is 1 and average flux through face $x = \mp a$ vanishes. The Raviart-Thomas space has these 2 degrees of freedom, and in terms of its nodal basis, it is

$$V_{E,d}^x = Q_{1,0,0} = \text{span}\{R_x^-,\ R_x^+\}.$$

A transition element E is a Darcy element that abuts a Stokes element at Γ. If two elements abut along the x-direction, the x-component of the transition space is a mixture of $V_{E,s}^x$ and $V_{E,d}^x$. In terms of its nodal basis, we define

$$V_{E,\pm}^x = \text{span}\{v_{\pm a,-b,-c},\ v_{\pm a,b,-c},\ v_{\pm a,-b,c},\ v_{\pm a,b,c},\ R_x^{\mp},\ B_x^{\pm}\},$$

which has 6 degrees of freedom: 2 average face flux degrees of freedom at $x = -a$ and $x = a$, and 4 corner degrees of freedom at $x = \pm a$ (and $y = -b, b$ and $z = -c, c$). In other words, we remove the corner degrees of freedom on face $x = \mp a$, and replace the bubble function by the Raviart-Thomas function.

We thus have 4 types of finite elements for x-components, as illustrated in Fig. 2.1, and analogous elements for y- and z-components. This results in 12 vector valued finite elements overall, which are

$$\mathbf{V}_{E,\alpha,\beta,\gamma} = V_{E,\alpha,}^x \times V_{E,\beta,}^y \times V_{E,\gamma,}^z,$$

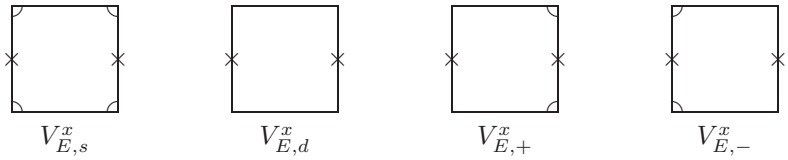

FIG. 2.1. *The degrees of freedom for the 4 types of elements for x-velocities. The times symbol, $\times$, represents the average face flux, and the quarter circles represent corner values. The first is used on Ω_s, while all four may be used on Ω_d.*

where α, β, and γ are one of s, d, or $\pm$, having from 6 to 30 degrees of freedom.

REMARK 2.1. *In* [2]*, in two dimensions, several more transition elements were defined. In each coordinate direction, there are 16 types, because one is allowed to keep 0, 1, 2, 3, or all 4 corner degrees of freedom. (Up to symmetry, then, there are seven types of elements.) Here we have disallowed such freedom, and required the finite element to have 0, 4, or all 8 corner degrees of freedom (so as to reduce the number of corner degrees of freedom as much as possible). Because the case of 4 corner degrees of freedom requires them to all lie on the same face normal to the coordinate direction, we have only 4 types of elements (or, up to symmetry, only 3 types). This considerably simplifies the computer coding exercise. Of course, one could define the additional finite elements if one wished to allow more flexibility as in* [2].

2.2. The finite element method. Let us assume now that $\Omega \subset \mathbb{R}^3$ and that both Ω_s and Ω_d are unions of rectangles. Let $\mathcal{T}_h$ be a rectangular, conforming finite element partition of Ω with maximal mesh size h, such that each element is within Ω_s or Ω_d. We easily define

$$W_h = \text{span}\{w_E : E \in \mathcal{T}_h\} \subset W,$$

where w_E is simply the characteristic function of the element E (i.e., 1 on the element and 0 elsewhere).

We define now a nodal basis for our velocity finite element space $\mathbf{V}_h \subset \mathbf{V}$. It is somewhat difficult to describe it, however, so we will define x-components first. For $E \in \mathcal{T}_h$, let (if they exist), E_- be the element immediately to the left, and E_+ the element to the right (in the x-direction). Then the x-component of $\mathbf{v}_h \in \mathbf{V}_h$ satisfies

$$v_h^x|_E \in \begin{cases} V^x_{E,s} & \text{if } E \subset \Omega_s, \text{ or } E \subset \Omega_d \text{ and } E_- \cup E_+ \subset \Omega_s, \\ V^x_{E,+} & \text{if } E \subset \Omega_d, E_- \subset \Omega_d, \text{ and } E_+ \subset \Omega_s, \\ V^x_{E,-} & \text{if } E \subset \Omega_d, E_- \subset \Omega_s, \text{ and } E_+ \subset \Omega_d, \\ V^x_{E,d} & \text{otherwise.} \end{cases}$$

This way, we have corners on Darcy elements only when they abut Stokes elements on Γ. We have similar rules for y- and z-components. Alternatively, one can view the construction as follows. Use $\mathbf{V}_{E,s}$ on Stokes elements, $\mathbf{V}_{E,d}$ on Darcy elements, and add in corner degrees of freedom on Darcy elements from $V_{E,-}$ or $V_{E,+}$ when necessary, i.e., when flow travels from Darcy to Stokes, or vice versa.

Now the definition of $\mathbf{V}_h \subset \mathbf{V}_0$ is clear: we choose our local elements as above, and match corner and face degrees of freedom. Normal components are always continuous, so $\mathbf{V}_h \subset H(\text{div};\Omega)$. Moreover, since we maintain corner degrees of freedom in the Stokes domain, $\mathbf{V}_h \subset H^1(\Omega_s)$, as required. By imposing the outer boundary

conditions, i.e., by removing normal degrees of freedom on Γ_N and all tangential degrees of freedom, we have our space. Further, $\mathbf{V}_{h,u_N}$ is given by setting the normal degrees of freedom appropriately.

For our finite element method, we seek $\mathbf{u}_h \in \mathbf{V}_{h,u_N}$ and $p_h \in W_h$ such that, for all $\mathbf{v}_h \in \mathbf{V}_h$ and $w_h \in W_h$,

$$\begin{aligned} 2\mu(D\mathbf{u}_h, D\mathbf{v}_h)_{\Omega_s} + \sum_{k=1}^{2} \mu(\alpha K^{-1/2}\mathbf{u}_{h,s}\cdot\tau_k, \mathbf{v}_{h,s}\cdot\tau_k)_\Gamma \\ + \mu(K^{-1}\mathbf{u}_h, \mathbf{v}_h)_{\Omega_d} - (p_h, \nabla\cdot\mathbf{v}_h)_\Omega = (g, \mathbf{v}_h)_\Omega - (p_D, \mathbf{v}_h\cdot\nu)_{\Gamma_D} \end{aligned} \tag{2.3}$$

$$(\nabla\cdot\mathbf{u}_h, w_h)_\Omega = (f, w_h)_\Omega. \tag{2.4}$$

By restricting to the basis finite elements, these discrete equations result is a symmetric system of linear equations of *saddle-point* form (1.11), where

$$\begin{aligned} A_{i,j} &= 2\mu(D\mathbf{v}_h^j, D\mathbf{v}_h^i)_{\Omega_s} + \sum_{k=1}^{2} \mu(\alpha K^{-1/2}\mathbf{v}_{h,s}^j\cdot\tau_k, \mathbf{v}_{h,s}^i\cdot\tau_k)_\Gamma \\ &\quad + \mu(K^{-1}\mathbf{v}_h^j, \mathbf{v}_h^i)_{\Omega_d}, \end{aligned} \tag{2.5}$$

$$B_{i,j} = -(w_h^j, \nabla\cdot\mathbf{v}_h^i)_\Omega, \tag{2.6}$$

$$g_i = (g, \mathbf{v}_h^i)_\Omega - (p_D, \mathbf{v}_h^i\cdot\nu)_{\Gamma_D}, \tag{2.7}$$

$$f_i = -(f, w_h^i)_\Omega. \tag{2.8}$$

Since Γ is restricted to grid lines, at least one of the three terms that appear in the formula for $A_{i,j}$ vanishes. To make a rough estimate of the order of magnitude of these terms, note that in the CGS unit system, $\mu \approx 10^{-2}$, $\alpha \approx 1$ and $K \approx 10^{-10}$. For our finite elements, the derivatives of $\mathbf{v}_h^i \sim h^{-1}$, so in dimension d,

$$\begin{aligned} \mu(D\mathbf{v}_h^j, D\mathbf{v}_h^i)_{\Omega_s} &\sim \mu h^{d-2} &&\sim 10^{-2}h^{d-2}, \\ \mu(\alpha K^{-1/2}\mathbf{v}_{h,s}^j\cdot\tau, \mathbf{v}_{h,s}^i\cdot\tau)_\Gamma &\sim \mu\alpha K^{-1/2}h^{d-1} &&\sim 10^{3}h^{d-1}, \\ \mu(K^{-1}\mathbf{v}_h^j, \mathbf{v}_h^i)_{\Omega_d} &\sim \mu K^{-1}h^{d} &&\sim 10^{8}h^{d}. \end{aligned}$$

These would be comparable if $h \sim 10^{-5}\,\mathrm{cm}$; however, one would not normally expect such a fine grid, since this would be below the pore scale (of perhaps $10^{-2}\,\mathrm{cm}$) and Darcy's law would not be expected to hold. Rather, $h \sim 1\,\mathrm{cm}$ is expected, so there are large variations in the sizes of the matrix elements of A, and one should expect that the linear system (1.11) is very ill-conditioned.

The condition number of matrix A for different systems is shown in Table 2.1. The domain is $8\,\mathrm{cm} \times 8\,\mathrm{cm} \times 4\,\mathrm{cm}$ and the mesh size is $h = 1\,\mathrm{cm}$. We include five cases: (1) a Darcy domain with uniform permeability of 1 md, (2) a heterogeneous Darcy domain with a permeability variation of 4 orders of magnitude, (3) a Stokes domain (using only a 4 cm cube domain), (4) a Darcy-Stokes system with a heterogeneous Darcy subdomain with an isolated vug, and (5) a Darcy-Stokes system with a heterogeneous Darcy subdomain and a connected vug. Notice the large condition number of matrix A for vuggy systems, and how much larger it is than for both simply heterogeneous porous media and pure Stokes systems.

2.3. Convergence of the finite element method. An optimal order convergence result for the two dimensional version of (2.3)–(2.4) was proved in [2]. All the

TABLE 2.1
Condition number of matrix A for different types of systems.

Type of system	Matrix size	Condition number
Darcy homogeneous	896 × 896	9.9124e+03
Darcy heterogeneous	896 × 896	8.3731e+05
Stokes only	615 × 615	2.1497e+07
Darcy-Stokes (isolated vug)	968 × 968	3.7116e+11
Darcy-Stokes (connected vug)	998 × 998	6.8248e+11

arguments can be readily extended to the three dimensional case (see also [5]), and we have the following theorem. For the notation, $\|\cdot\|_{m,l}$ denotes the usual norm in the Sobolev space $H^m(\Omega_l)$, for $m = 1, 2$ and $l = s, d$, and $\|\cdot\|_{0,l}$ is the $L^2(\Omega_l)$ norm. Also, $\mathcal{P}_W : L^2(\Omega) \to W_h$ denotes the L^2 projection operator.

THEOREM 2.1. *Assume that the solution* $(\mathbf{u}, p)$ *and data of* (2.1)–(2.2) *is sufficiently smooth so that all the norms that appear below are finite. Then, there is a constant* C *such that*

$$\begin{aligned}\|\mathbf{u} - \mathbf{u}_h\|_{1,s} + \|\mathbf{u} - \mathbf{u}_h\|_{0,d} + \|p - p_h\|_0 \\ \leq Ch(\|g\|_{1,d} + \|\mathbf{u}\|_{2,s} + \|\mathbf{u}\|_{1,d} + \|p\|_{1,s} + \|p\|_{1,d} + \|p_D\|_{1,\Gamma_D}).\end{aligned} \tag{2.9}$$

Moreover, $\mathcal{P}_W \nabla \cdot \mathbf{u}_h = \mathcal{P}_W f$.

3. A multigrid solver for the discretized system. For ease of exposition, we present this part of the work in two dimensions, although it easily generalizes to three dimensional flows. For a detailed treatment of multigrid methods, we refer the reader to [28, 9, 18]. In the next subsection, which the experts can skip, we present the main ideas of multigrid.

3.1. A review of multigrid. Suppose we want to solve the system

$$L_h x = b, \tag{3.1}$$

where matrix L_h represents the discretized version of a partial differential operator with certain boundary conditions, and x and b are the finite element basis coefficients of functions defined on a certain grid G_h with mesh size h.

Most iterative methods efficiently reduce the high frequency components of the error $x - x^n$, where x^n is the approximation to x obtained after the nth iteration. However, they do not remove the low frequency components. If we try to solve (3.1) using such a smoothing procedure, we will observe that, after a number of iterations, the reduction in the magnitude of the error becomes very small. In order to overcome this difficulty, we need a better method to eliminate the slow components of the error. We observe that the notion of high frequency or low frequency for a function defined on a grid depends on the mesh size. A grid function which is "slow" relative to a grid with mesh size h becomes a relatively faster signal when restricted to a subgrid with mesh size $2h$.

Suppose now that we apply a number of smoothing iterations and obtain an approximation x_h to the exact solution x of (3.1). If y solves the residual equation

$$L_h y = r_h = b - L_h x_h, \tag{3.2}$$

then $x_h + y = x$ is the exact solution of (3.1). We also know that high frequency components have been removed from the error $x - x_h$, so $y = x - x_h$ should contain

only slow components (relative to grid G_h). Thus, we "solve" (3.2) on a coarser grid with mesh size, say, $2h$. Let G_{2h} be such a grid. We need to define some version of the operator L_h for grid G_{2h}. Denote this new operator by L_{2h}. We also need to define the right hand side for the new equation. To this end we define a restriction operator R_h^{2h}. The residual equation posed on grid G_{2h} reads

$$L_{2h}y_{2h} = R_h^{2h}r_h, \tag{3.3}$$

where the unknown y_{2h} is obviously a function defined on grid G_{2h}.

Once we solve equation (3.3), we need to add this coarse-grid correction to x_h, but first, we need to prolongate y_{2h} to a function defined on G_h. Define a prolongation operator P_{2h}^h, and then a better approximation to x should be given by

$$x_h' = x_h + P_{2h}^h y_{2h}.$$

It turns out that we do not need to solve (3.3) exactly, we just need an approximate solution. Therefore we can now follow the same steps we did before: we first apply a number of smoothing iterations on G_{2h} and then we solve the residual equation on G_{4h} and so on, until we reach a sufficiently coarse grid, where an exact solver can be applied inexpensively.

According to the discussion above, in order to design a multigrid algorithm we need to specify: (1) the type of cycle, (2) the grid coarsening strategy, (3) the inter-grid transfer operators (restriction and prolongation operators), (4) the coarse grid operators, and (5) the smoothing procedure. We will now explain our choices. The most important aspect is choosing the smoother and prolongation operators.

3.2. Cycle type and coarsening strategy. For the type of cycle, we use V-cycles, since we found a better balance between the convergence rate and the computational work for these types of schemes than for W-cycles.

For simplicity, we tacitly assume that $\mathcal{T}_h$ is a uniform square grid of spacing h. Let $G^M = \mathcal{T}_h$ denote the finest grid. Actually, G^M denotes the nodal points where the solution $(u, p) = (u_x, u_y, p)$ of (1.11) is defined (see Fig. 3.1). Then $G^M = G_x^M \cup G_y^M \cup G_p^M$, where G_x^M, G_y^M, G_p^M are subgrids of G^M where u_x, u_y, and p are defined, respectively. (Although the degrees of freedom corresponding to the fluxes are defined on edges, we will identify an edge with its midpoint, as the figure shows. Also, we identify each cell where the pressure is defined with its center point.) More precisely, G_x^M consists of the corner points $\{(ih, jh)\}$ and the edge points $\big\{(ih, (j + 1/2)h)\big\}$. Similarly, G_y^M contains $\{(ih, jh)\}$ and $\big\{((i+1/2)h, jh)\big\}$, and G_p^M is $\big\{((i+1/2)h, (j+1/2)h)\big\}$.

Let $G^{M-1}, ..., G^0$ denote a sequence of successively coarser grids constructed from G^M as follows. First, G^{M-1} is obtained from G^M by removing the corner points, so G^{M-1} also has mesh size h. We also have $G^{M-1} = G_x^{M-1} \cup G_y^{M-1} \cup G_p^{M-1}$, where G_x^{M-1} and G_y^{M-1} are obtained from G_x^M and G_y^M, respectively, by removing the corners, and $G_p^{M-1} = G_p^M$.

Given grid G^k, $k = M - 1, M - 2, ..., 1$, each cell of grid G^{k-1} consists of 4 neighboring cells of grid G^k, so we coarsen the grid by doubling the mesh size. In the same way we had for G^k, for each cell of G^{k-1} we have a grid point at the center of the cell where pressure is defined and the midpoint of each edge where velocity fluxes are defined (see Fig. 3.2). For every $k = M, M-1, ..., 0$, we have $G^k = G_x^k \cup G_y^k \cup G_p^k$, where the definitions of these non-nested subgrids of G^k are now obvious from the previous

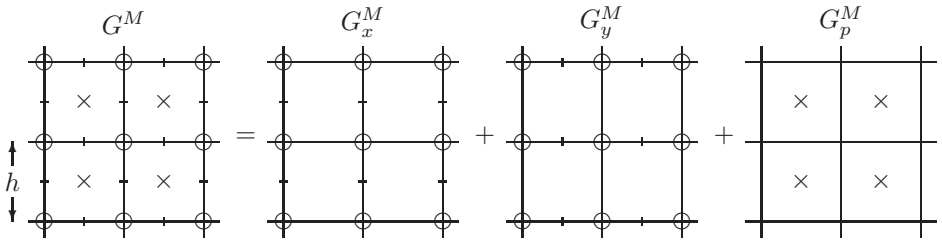

FIG. 3.1. *The finest grid $G^M = G_x^M \cup G_y^M \cup G_p^M$. Velocities in the x- and y-direction are defined at corners of elements. Average fluxes are defined on edges. Pressure is constant on each element.*

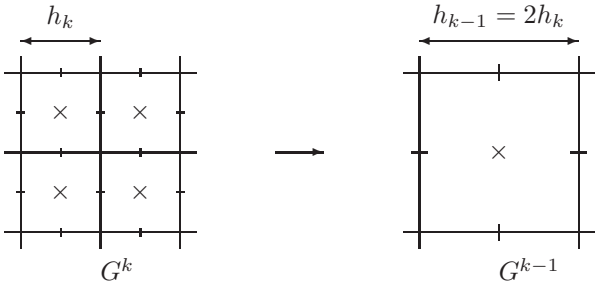

FIG. 3.2. *Grid coarsening for $k = M-1, M-2, ..., 1$.*

discussion. That is, for $k < M$, $h_k = 2^{M-k-1}h$ and G_x^k is $\{(ih_k, (j+1/2)h_k)\}$, G_y^k is $\{((i+1/2)h_k, jh_k)\}$, and G_p^k is $\{((i+1/2)h_k, (j+1/2)h_k)\}$.

Notice that this coarsening strategy preserves the cell structure of the finest grid (except for the corners), which allows us to think of the unknown quantities defined on coarser grids as cell pressures and edge average fluxes per unit length. This way of thinking will guide us in the design of the prolongation and restriction operators.

3.3. Intergrid prolongation operators. For each $k = M, M-1, ..., 0$, let V_x^k, V_y^k, and V_p^k denote the set of real valued functions defined on grids G_x^k, G_y^k, and G_p^k, respectively, and let $V^k = V_v^k \times V_p^k$, where $V_v^k = V_x^k \times V_y^k$. We need to define the prolongation

$$P^k : V^{k-1} \to V^k, \quad k = 1, 2, ..., M-1. \tag{3.4}$$

We will define P^k in such a way that $P^k(u,p) = (P_v^k u, P_p^k p)$, where $P_v^k : V_v^{k-1} \to V_v^k$ and $P_p^k : V_p^{k-1} \to V_p^k$. In matrix notation, P^k will be block diagonal,

$$P^k = \begin{bmatrix} P_v^k & 0 \\ 0 & P_p^k \end{bmatrix}, \tag{3.5}$$

so that prolongation does not mix velocities and pressures.

We need to distinguish cases $k = M$ and $k < M$.

3.3.1. Definition of the prolongation when $k = M$. Since $G_p^M = G_p^{M-1}$, we simply set P_p^M to be the identity operator on $V_p^{M-1} = V_p^M$.

Now let $u \in V_v^{M-1}$, and let $P_v^M u = w = (w_x, w_y) \in V_v^M$ be defined as follows. Recall that G_v^{M-1} comes from G_v^M by deleting the corners. We let P_v^M be the identity

on the face degrees of freedom. That is, if $t = (ih, (j+1/2)h) \in G_x^M \setminus G_y^M$ (i.e., not a corner point), then we set $w_x(t) = u_x(t)$. Similarly, if $t = ((i+1/2)h, jh) \in G_y^M \setminus G_x^M$, then we set $w_y(t) = u_y(t)$.

For a corner $t = (ih, jh) \in G_x^M \cap G_y^M$, we have two possibilities. If the 4 elements that share the corner t are Stokes elements, i.e., they are contained in Ω_s, then we do not expect to find jumps in the solution. We recall that the order of the interpolation should be at least the order of the differential operator minus 1 [9], so we use linear interpolation. Thus we define

$$w_x(ih, jh) = \frac{1}{2}\big(u_x(ih, (j-1/2)h) + u_x(ih, (j+1/2)h)\big),$$
$$w_y(ih, jh) = \frac{1}{2}\big(u_y((i-1/2)h, jh) + u_y((i+1/2)h, jh)\big).$$

The second possibility is that at least one of the four elements that has t as a corner is a Darcy element, in which case we simply set

$$w_x(t) = w_y(t) = 0.$$

We remark that, based on the physical considerations of a simple model problem in the next subsection, the tangential velocity on the Darcy-Stokes interface is approximately 10^4 times smaller than the flux per unit length in the Stokes domain (see (3.7) below). Based on this argument, if, say, the top 2 elements were Stokes, we should have set, say, $w_x(t) = 10^{-4}u_x(ih, (j+1/2)h)$. However, in practice we saw very little difference between this and simply taking $w_x(t) = 0$.

3.3.2. Physical considerations and element edge classification. The correct design of the prolongation operators for $k < M$ turns out to be an important factor in obtaining a convergent multigrid algorithm. From a physical point of view, the problem is that the medium contains vug channels that support very high flow rates. This makes prolongation difficult. In order to gain some insight about the orders of magnitude of the velocity on the Stokes and Darcy subdomains, we analyze at the following simple model case. Consider a Darcy-Stokes system that consists of a channel of width l limited above and below by a porous medium (see Fig. 3.3). The flow in the channel satisfies the Stokes equation, and the flow in the porous medium obeys Darcy's law.

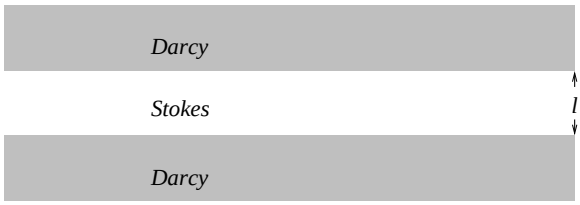

FIG. 3.3. *A Darcy-Stokes system with a central channel limited by porous rock.*

Assume that we have a constant pressure gradient, $-\delta p$, in the x-direction, that the flow is stationary, and that the channel is infinitely long in the x-direction, so that the velocity field does not depend on the x-coordinate. (Although the action of the prolongation operator we will construct is local, these assumptions and our model case will prove useful for our purposes.) Let $u(y)$ denote the velocity of the fluid in

the x-direction. The Stokes equation for the velocity field in the channel and the Beavers-Joseph-Saffman boundary condition take the form

$$\begin{aligned} -\mu u''(y) - \delta p &= 0, \\ u'(0) &= \alpha K^{-1/2} u(0), \\ u'(l) &= -\alpha K^{-1/2} u(l), \end{aligned}$$

and the solution is

$$u(y) = \left(-\frac{1}{2\mu} y^2 + \frac{l}{2\mu} y + \frac{l K^{1/2}}{2\mu\alpha} \right) \delta p.$$

The average velocity in the channel is $\bar{u}_s = \dfrac{1}{l} \displaystyle\int_0^l u(y)\, dy = \left(\frac{l K^{1/2}}{2\mu\alpha} + \frac{l^2}{12\mu} \right) \delta p.$ On the other hand, Darcy's law implies that $u_d = \dfrac{K}{\mu} \delta p$. Thus, the ratio of average Stokes to Darcy flow is

$$\frac{\bar{u}_s}{\bar{u}_d} = \frac{l}{2\alpha K^{1/2}} + \frac{l^2}{12K} \approx \frac{l^2}{12K} \approx 10^8, \tag{3.6}$$

assuming $\alpha \approx 1$, $K \approx 10^{-10}\,\mathrm{cm}^2$ and $l \approx 0.3\,\mathrm{cm}$. Moreover, the velocity on the interface is $u(0) = u(l) = \dfrac{l K^{1/2}}{2\mu\alpha} \delta p$, so

$$\frac{\bar{u}_s}{u(0)} = 1 + \frac{l\alpha}{6K^{1/2}} \approx \frac{l\alpha}{6K^{1/2}} \approx 10^4. \tag{3.7}$$

That is, the flow in the Stokes channel dominates, being about 10^8 times larger than that in the porous medium and 10^4 times larger than the velocity on Γ.

However, this large difference in velocities are not expected when the vugs do not form channels. Such disconnected vugs, i.e., a region of adjacent Stokes elements completely surrounded by Darcy elements, must be treated more like the Darcy region. We thus classify the edges on each grid according to the magnitude of the flux that we expect to observe.

We begin on the finest grid G^M. If an edge is shared by at least one Darcy element, then we expect the flow through this edge to be relatively small, and we say that this is a D-edge. If an edge is shared by two Stokes elements, then it may be part of a channel, with relatively large flow, or it may be within a disconnected vug. So we first label every edge that has two adjacent Stokes elements as an S-edge. Then we run a few smoothing iterations on the finest-grid, which will be enough for us to get an idea of the order of magnitude of the flux through every edge. If after a few smoothing iterations, the flux through an S-edge is "small" (less than, say, 10^{-1} times the expected channel flow), then we relabel it as an S-d-edge.

On coarser grids G^k ($k < M-1$), if an edge contains at least one finest-grid edge of type S, then we label it as an edge of type S. If an edge is not of type S and it contains at least one finest grid edge of type S-d, then we say that it is an S-d-edge. Finally, an edge on a coarser grid which consists only of finest-grid D-edges will be a D-edge. In this way, we obtain an estimate of the global channeling behavior of the medium, which we will exploit in the prolongation.

3.3.3. Definition of the prolongation when $k < M$. We now consider the case $k < M$. To prolongate the pressure, if $q \in V_p^{k-1}$, we set the finer grid pressures equal to the coarse grid pressure; that is, we define (see Fig. 3.4)

$$P_p^k q(c_\ell) = q(c), \quad \ell = 1, 2, 3, 4, \tag{3.8}$$

where $c_\ell \in \{((i \pm 1/2)h_k, (j \pm 1/2)h_k)\}$ and $c = (ih_k, jh_k)$. The mapping P_p^k is clearly injective.

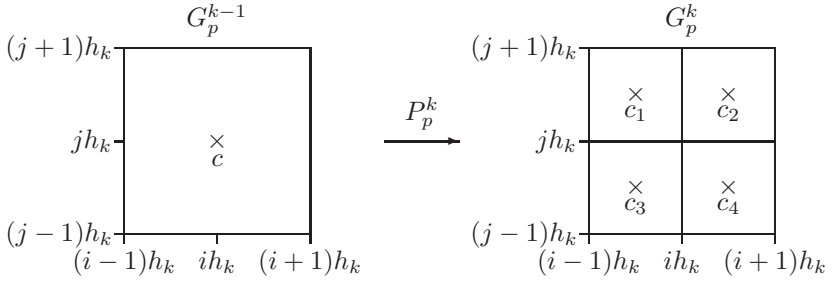

FIG. 3.4. *Pressure prolongation from G_p^{k-1} to G_p^k, $k < M$. The pressure in each of the 4 finer cells is set equal to the pressure in the coarser-grid cell.*

Let $u = (u_x, u_y) \in V_v^{k-1}$ and let $P_v^k u = w = (w_x, w_y) \in V_v^k$. According to Fig. 3.5, u is defined on the coarser-grid edges e_1, e_2, e_3, and e_4, and we should define w on the finer-grid edges $\{e_{i\pm}\}_{i=1,\ldots,6}$.

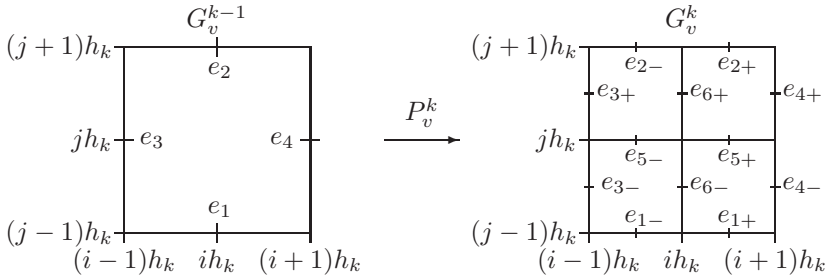

FIG. 3.5. *Velocity prolongation for $k < M$. If $w = P_v^k u$, then u is defined on e_1, e_2, e_3, and e_4, and w is defined on $\{e_{i\pm}\}_{i=1,\ldots,6}$.*

We first define w_x on the coarse grid boundaries $e_{4\pm} = ((i+1)h_k, (j \pm 1/2)h_k)$, using only u_x on $e_4 = ((i+1)h_k, jh_k)$ for consistency between elements. If we assume that u and w approximately describe average fluxes, then

$$2h_k u_x(e_4) \approx h_k\big(w_x(e_{4+}) + w_x(e_{4-})\big).$$

According to the discussion in the previous subsection, the orders of magnitude of $w_x(e_{4+})$ and $w_x(e_{4-})$ should be in the ratio

$$\frac{w_x(e_{4+})}{w_x(e_{4-})} \approx \phi_4 = \phi(e_{4+}, e_{4-}),$$

where

$$\phi(\varepsilon_1,\varepsilon_2)=\begin{cases}1 & \text{if } \varepsilon_1 \text{ and } \varepsilon_2 \text{ are edges of the same type,}\\ \dfrac{h_k^2}{12K}\approx 10^8 & \text{if } \varepsilon_1 \text{ is an S-edge and } \varepsilon_2 \text{ is a D-edge or S-d-edge,}\\ \dfrac{12K}{h_k^2}\approx 10^{-8} & \text{if } \varepsilon_1 \text{ is an D-edge or S-d-edge and } \varepsilon_2 \text{ is a S-edge,}\\ 10 & \text{if } \varepsilon_1 \text{ is an S-d-edge and } \varepsilon_2 \text{ is an D-edge,}\\ 0.1 & \text{if } \varepsilon_1 \text{ is an D-edge and } \varepsilon_2 \text{ is an S-d-edge.}\end{cases} \tag{3.9}$$

The latter two cases might be set to 1, but empirically we found that the above choice gave good practical results, although convergence is not particularly sensitive to this choice. We therefore define

$$w_x(e_{4+})=\frac{2}{1+\phi_4^{-1}}u_x(e_4) \quad \text{and} \quad w_x(e_{4-})=\frac{2}{1+\phi_4}u_x(e_4).$$

We similarly define $w_x(e_{3\pm})$, $w_y(e_{1\pm})$, and $w_y(e_{2\pm})$. That is, in general,

$$w_x(\varepsilon_\pm)=\frac{2}{1+\phi(\varepsilon_\mp,\varepsilon_\pm)}u_x(\varepsilon) \quad \text{and} \quad w_y(\varepsilon_\pm)=\frac{2}{1+\phi(\varepsilon_\mp,\varepsilon_\pm)}u_y(\varepsilon). \tag{3.10}$$

Note that (3.10) implies that P_v^k is injective. Since P_p^k is also injective, P^k itself is injective.

We now define our prolongation in the interior of the course element at $e_{5\pm}=((i\pm1/2)h_k,jh_k)$ and $e_{6\pm}=(ih_k,(j\pm1/2)h_k)$ (see Fig. 3.5). Let e_6 denote the union of edges e_{6-} and e_{6+}. If there are no sources inside the element, then an approximation of the total flux through e_6 is given by the average of the fluxes that enter the element through edges e_3, e_{2-} and e_{1-}, and exit the element through edges e_{1+}, e_{2+}, and e_4. Let $u_x(e_6)$ denote this flux, which is then

$$u_x(e_6)=\frac{1}{4}\big[2u_x(e_3)+w_y(e_{1-})-w_y(e_{2-})+2u_x(e_4)+w_y(e_{2+})-w_y(e_{1+})\big]. \tag{3.11}$$

We now use (3.10) to distribute the flux over the finer edges. Similarly, we define

$$u_y(e_5)=\frac{1}{4}\big[2u_y(e_1)+w_x(e_{3-})-w_x(e_{4-})+2u_y(\mathbf{e}_2)-w_x(e_{3+})+w_x(e_{4+})\big], \tag{3.12}$$

and then $w_y(e_{5\pm})$ from (3.10).

In summary, our prolongation operator is designed to prolongate fluxes in a physically appropriate way. As we noted, the difficulty is that vuggy media tend to contain Stokes channels with high flow rates. Our prolongation tries to recognize this fact. Initial smoothing identifies the channels. High fluxes in Stokes channels across coarse edges are prolongated in such a way that they are biased to the side containing the Stokes elements, and away from Darcy elements. This preserves the channeling structure throughout the multigrid procedure and improves convergence.

3.4. Restriction and coarse-grid operators. We need to define the analog of (1.11) for each grid. One possible choice is to consider the finite element space associated to the corresponding elements or cells. However, it has the serious disadvantage that the functions of these finite element spaces are continuous in the interior of every element. A discontinuity on a segment of the Darcy-Stokes interface contained in the

interior of an element would not be allowed on coarser grids. Therefore, we will use the so called Galerkin coarse grid approximation, where the discrete operator for level k is recursively given by

$$L_k = (R^k)^t L_{k+1} P^{k+1}, \quad k = M-1, M-2, ..., 0, \tag{3.13}$$

where L_M is given by (1.11) and R^k is the intergrid restriction operator.

To maintain symmetry of the coarse-grid operators, we set

$$R^k = (P^{k+1})^t : V^{k+1} \to V^k, \quad k = M-1, M-2, ..., 0. \tag{3.14}$$

LEMMA 3.1. *Let L_M be the matrix of system* (1.11)*, and set $A^M = A$ and $B^M = B$, where A and B are given by* (2.5)–(2.6)*. For each $k = M-1, ..., 0$, let L_k be the discrete operator given by* (3.13)*. Then L_k, $k = M, M-1, ..., 0$, has the form*

$$L_k = \begin{bmatrix} A^k & B^k \\ (B^k)^t & 0 \end{bmatrix}, \tag{3.15}$$

where A^k is symmetric and positive definite. Moreover, when $k < M$,

$$A^k = (P_v^{k+1})^t A^{k+1} P_v^{k+1}, \tag{3.16}$$

$$B^k = (P_v^{k+1})^t B^{k+1} P_p^{k+1}. \tag{3.17}$$

Proof. Because prolongation (3.5) does not mix velocities and pressures, it is easy to compute successively from (3.13) that

$$\begin{aligned} L_k &= (P^{k+1})^t L_{k+1} P^{k+1} \\ &= \begin{bmatrix} (P_v^{k+1})^t & 0 \\ 0 & (P_p^{k+1})^t \end{bmatrix} \begin{bmatrix} A^{k+1} & B^{k+1} \\ (B^{k+1})^t & 0 \end{bmatrix} \begin{bmatrix} P_v^{k+1} & 0 \\ 0 & P_p^{k+1} \end{bmatrix} = \begin{bmatrix} A^k & B^k \\ (B^k)^t & 0 \end{bmatrix}, \end{aligned}$$

as claimed, with (3.16)–(3.17) holding. Clearly (2.5) shows that $A = A^M$ is positive definite. Since P_v^k is injective, A^k is also positive definite for each $k = M-1, ..., 0$. ∎

3.5. Smoothing procedure. The difficulty in finding a good smoother for (1.11) is that the system, as we saw earlier, is extremely ill-conditioned. We present here a new smoother that has worked well for our problem. In order to abbreviate the notation, we explain the smoothing procedure for the finest grid. Because of (3.15), everything is valid for coarser grids, except for minor differences that we will mention below.

Suppose we have computed an approximation (u^n, p^n) to the solution (u, p) of system (1.11), and we want to compute a better approximation (u^{n+1}, p^{n+1}) by smoothing the error. The first step of our method is to find the *directions* along which we should modify (u^n, p^n). In other words, we try to find *optimal* vectors ψ and ϕ to define (u^{n+1}, p^{n+1}) as

$$\begin{aligned} u^{n+1} &= u^n + \beta\psi, \\ p^{n+1} &= p^n + \alpha\phi, \end{aligned} \tag{3.18}$$

for appropriate values of α and β that will be determined in the second step of our procedure.

If ψ and ϕ are "good directions," it is reasonable that they should approximate the errors $\psi = u - u^n$ and $\phi = p - p^n$, and therefore can be obtained by computing an approximate solution of

$$\begin{bmatrix} A & B \\ B^t & 0 \end{bmatrix} \begin{bmatrix} \psi \\ \phi \end{bmatrix} = \begin{bmatrix} r^n \\ s^n \end{bmatrix}, \tag{3.19}$$

where r^n and s^n are the residuals

$$r^n = g - Au^n - Bp^n, \tag{3.20}$$

$$s^n = f - B^t u^n. \tag{3.21}$$

We obtain an approximate solution of (3.19) using the Uzawa algorithm [7, 8]. Let $\hat{A}^{-1}$ be a preconditioner, or approximate inverse, of A, such as given by taking $\hat{A} = \mathrm{diag}(A)$ (i.e., $\hat{A}$ is diagonal and $\hat{A}_{ii} = A_{ii}$ for all indexes i). Also let C^{-1} be a preconditioner for $B^t A^{-1} B$, such as $C = \mathrm{diag}(B^t \hat{A}^{-1} B)$ (we return to this choice near the end of this subsection). Then Uzawa iterations, indexed by ℓ, are given by

$$\psi^{\ell+1} = \psi^\ell + a\hat{A}^{-1}(r^n - A\psi^\ell - B\phi^\ell), \tag{3.22}$$

$$\phi^{\ell+1} = \phi^\ell + bC^{-1}(B^t\psi^{\ell+1} - s^n), \tag{3.23}$$

where $a, b > 0$ are damping parameters. We generally obtained good results with $a = b$ between 0.4 and 0.8. We note that if $\hat{A}^{-1}$ and C^{-1} were exact preconditioners, the scheme would converge in very few iterations. We perform a number L of Uzawa iterations starting with $\psi^0 = 0$ and $\phi^0 = 0$, and set $\psi = \psi^L$ and $\phi = \phi^L$. The value for L is problem dependent. We obtained good results with L between 5 and 40 for the problems we solved.

Once we have computed ψ and ϕ, the second step of our smoothing procedure is to find optimal values for α and β in (3.18). We search for the values of α and β that minimize the residuals corresponding to the $(n+1)th$ iteration. More precisely, we minimize

$$R = w_u|r^{n+1}|^2 + w_p|s^{n+1}|^2,$$

where $w_u = 1/(1 + |u^n|^2)$ and $w_p = 1/(1 + |p^n|^2)$ are weights used to normalize the residuals. Notice that (3.18) implies

$$r^{n+1} = r^n - \alpha B\phi - \beta A\psi,$$
$$s^{n+1} = s^n - \beta B^t\psi,$$

so α and β will be the solutions of the pair of linear equations

$$w_u(r^n - \alpha B\phi - \beta A\psi) \cdot B\phi = 0,$$
$$w_u(r^n - \alpha B\phi - \beta A\psi) \cdot A\psi + w_p(s^n - \beta B^t\psi) \cdot B^t\psi = 0.$$

The determinant of the matrix is

$$D = \frac{w_p}{w_u}|B\phi|^2|B^t\psi|^2 > 0,$$

so

$$\alpha = \frac{1}{D}\left\{ \left(\frac{w_p}{w_u}|B^t\psi|^2 + |A\psi|^2\right) r^n \cdot B\phi - A\psi \cdot B\phi \left(r^n \cdot A\psi + \frac{w_p}{w_u} s^n \cdot B^t\psi\right)\right\}, \tag{3.24}$$

$$\beta = \frac{1}{D}\left\{ -(B\phi \cdot A\psi)(r^n \cdot B\phi) + |B\phi|^2 \left(r^n \cdot A\psi + \frac{w_p}{w_u} s^n \cdot B^t\psi\right)\right\}. \tag{3.25}$$

We summarize our smoothing procedure. Given an approximation (u^n, p^n), we first find directions ψ and ϕ by running a few Uzawa iterations for system (3.19). Then we compute α and β using formula (3.24)–(3.25), and finally we define (u^{n+1}, p^{n+1}) as given by (3.18).

We suggested above a simple diagonal preconditioner $C^{-1} = (\mathrm{diag}(B^t \hat{A}^{-1} B))^{-1}$ for $B^t A^{-1} B$, which is efficient to apply but not very effective for our highly ill-conditioned system. We can improve this preconditioner by applying it in a Jacobi type iteration. That is, when we wish to solve $B^t A^{-1} B v = w$ for v, we compute it from several iterations (generally from 5 to 40) of

$$v^{m+1} = v^m + (\mathrm{diag}(B^t \hat{A}^{-1} B))^{-1}(w - B^t \hat{A}^{-1} B v^m), \tag{3.26}$$

which is still quite efficient, since we use $\hat{A}$ in place of A. That is, we precondition $B^t \hat{A}^{-1} B$ with $(\mathrm{diag}(B^t \hat{A}^{-1} B))^{-1}$ in a Jacobi iteration.

Regular Uzawa sometimes does not smooth our Darcy-Stokes system when either the original or modified preconditioner for $B^t A^{-1} B$ is used. However, our two step Uzawa procedure is much more robust. It sometimes smooths when $C = \mathrm{diag}(B^t \hat{A}^{-1} B)$, and generally always smooths (for appropriate choices of parameters) when the Jacobi type C^{-1} is used. That is, our two step Uzawa procedure is valuable when we do not have a very good preconditioner for $B^t A^{-1} B$, which is necessarily true for the three dimensional Darcy-Stokes system.

As we mentioned above, since the coarser grid systems also have a saddle point structure (see (3.15)), our smoothing method is valid for every grid by replacing A by A^k and B by B^k. However, for the sake of efficiency, we apply the following minor modifications to the preconditioners, since it is inefficient to compute the diagonal of A^k for each level. If $k < M$ is the grid level, instead of using $\hat{A}^k = \mathrm{diag}(A^k)$, we use

$$\hat{A}^k = \begin{pmatrix} m_x I & 0 & 0 \\ 0 & m_y I & 0 \\ 0 & 0 & m_z I \end{pmatrix},$$

where, if we let A_x^k be the block of A^k corresponding to degrees of freedom in the x-direction, then

$$m_x = \max_i |A_{x,ii}|,$$

and similarly for the other blocks.

At every grid level, we stop performing smoothing iterations after we have performed at least a few (such as 4) iterations and when either the smoothing rate, given by the ratio between the l_2 norms of the residuals corresponding to two consecutive iterations, becomes larger than a prefixed value, or the norm of the residual becomes small enough. In our cases, the tolerance for the smoothing rate was 0.98 and the error tolerance for the residual norm was approximately 10^{-2}. As we explained in §3.1, when we stop the pre-smoothing, we move to the immediately coarser grid to find an approximate solution of the residual equation. When we stop post-smoothing, we prolongate our solution to the immediately finer grid and add it to the approximate solution that we have at this level.

3.6. Simplification of B^k. In this subsection, we show that the action of the operators $(B^k)^t$, $k = M, M-1, ..., 0$ are easily implemented, because they have a simple divergence structure made clear below.

Let $w_h^j : \Omega \to \mathbb{R}$ be the basis function equal to 1 on element E_j and 0 elsewhere. Let $\mathbf{v}_h^{i,e}$ be the basis function with unit average flux on edge e_i, and let $\mathbf{v}_h^{i,C}$ be the basis function with value 1 at corner C_i. Now the entries of matrix B (see (2.6)) have the form

$$\begin{aligned} B_{ij} = B_{ij}^M &= -(w_h^j, \nabla \cdot \mathbf{v}_h^{i,\xi})_{E_j} = -(w_h^j, \mathbf{v}_h^{i,\xi} \cdot \nu)_{\partial E_j} \\ &= \begin{cases} -h & \text{if } \xi = e \text{ and } E_j \text{ is located to the left of or below } e_i, \\ h & \text{if } \xi = e \text{ and } E_j \text{ is located to the right of or above } e_i, \\ 0 & \text{otherwise.} \end{cases} \end{aligned} \tag{3.27}$$

That is, B^t is a matrix of negative divergence type, in that it is constructed as

$$B^t u(c) = -h\big(u(e_2) - u(e_1) + u(e_4) - u(e_3)\big), \tag{3.28}$$

where (see Fig. 3.6) $c = ((i+1/2)h, (j+1/2)h)$, $e_1 = ((i+1/2)h, jh)$, $e_2 = ((i+1/2)h, (j+1)h)$, $e_3 = (ih, (j+1/2)h)$, and $e_4 = ((i+1)h, (j+1/2)h)$.

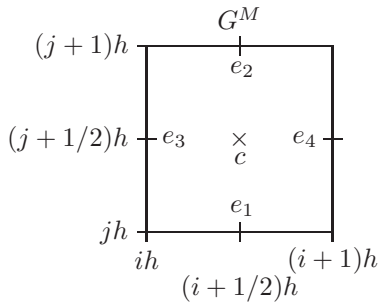

FIG. 3.6. *A typical cell of grid G^M.*

Now

$$B_{ij}^{M-1} = \sum_{m,k} (P_v^M)_{mi} B_{mk} (P_p^M)_{kj} = \sum_m (P_v^M)_{mi} B_{mj},$$

has the same form as (3.27), since P_p^M is the identity and P_v^M merely removes corners. That is, B^{M-1} is obtained from B by removing the identically vanishing rows that correspond to corner points of the finest grid, and so (3.27) holds for B^{M-1}, and $(B^{M-1})^t : V_v^{M-1} \to V_p^{M-1}$ is again the negative discrete divergence operator.

We have that $(B^k)^t : V_v^k \to V_p^k$ is the negative discrete divergence operator for $k = M$ and $k = M-1$, so let $k \le M-1$ and $u \in V_v^{k-1}$. Using the notation in Fig. 3.7 and the definitions of the matrices (3.17) and prolongation operators (3.8) and (3.10), we have by induction that

$$\begin{aligned} (B^{k-1})^t u(c) &= (P_p^k)^t (B^k)^t P_v^k u(c) \\ &= \sum_{i=1}^4 (B^k)^t P_v^k u(c_i) \\ &= -h_k \big[P_v^k u(e_{2-}) + P_v^k u(e_{2+}) - P_v^k u(e_{1-}) - P_v^k u(e_{1+}) \\ &\qquad - P_v^k u(e_{3-}) - P_v^k u(e_{3+}) + P_v^k u(e_{4-}) + P_v^k u(e_{4+}) \big] \\ &= -h_{k-1} \big(u(e_2) - u(e_1) - u(e_3) + u(e_4) \big), \end{aligned} \tag{3.29}$$

wherein we have used that the terms corresponding to internal edges in Fig. 3.7 cancel out because the contributions from the two elements that share each edge have opposite signs, and also that $2h_k = h_{k-1}$. Thus, we conclude that $(B^k)^t : V_v^k \to V_p^k$ is the negative discrete divergence operator for all $k = M, M-1, ..., 0$.

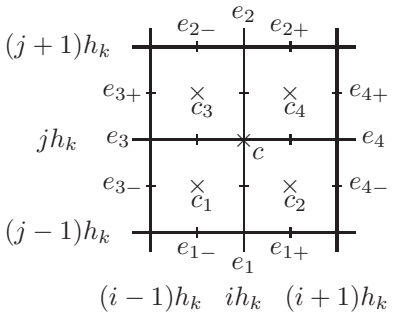

FIG. 3.7. *Finer grid G^k within coarser grid G^{k-1}.*

REMARK 3.1. *In general, it is not possible to construct A^k more simply than as given recursively in* (3.16). *However, we have shown that, in the natural basis of* §2.1, *each $(B^k)^t$ is easily constructed as a negative discrete divergence, and, conversely, each B^k is a discrete gradient. We used this observation to write a simpler and more efficient computer code to implement the multigrid procedure.*

3.7. Solvability. We now prove that the coarse-grid operators L_k given by (3.13) are nonsingular.

THEOREM 3.2. *Assume the hypotheses of Lemma* 3.1. *If $\Gamma_D \neq \emptyset$, then the system*

$$L_k x = c \tag{3.30}$$

has a unique solution $x \in V^k$ for any $c \in V^k$, for $k = M, M-1, ..., 0$. If $\Gamma_D = \emptyset$, then (3.30) *has a unique solution $x = (u, p)$ up to p being restricted to the space $V_p^k/\mathbb{R}$.*

Proof. Since L_k is a square, finite dimensional linear system, existence and uniqueness of a solution is equivalent to uniqueness at $c = 0$. In that case, for $x = (u, p)$, we have that

$$x^t L_k x = \begin{bmatrix} u^t A^k u + u^t B^k p \\ p^t (B^k)^t u \end{bmatrix} = \begin{bmatrix} 0 \\ 0 \end{bmatrix},$$

which implies that $u^t A^k u = 0$, since $u^t B^k p = p^t (B^k)^t u = 0$. Since A^k is symmetric, positive definite by Lemma 3.1, we have $u = 0$. Then $L_k(0, p) = 0$ implies that $B^k p = 0$.

We proceed with a standard argument. Consider the auxiliary elliptic problem

$$\begin{aligned} \nabla \cdot \psi &= p && \text{in } \Omega, \\ \psi &= -\nabla \phi && \text{in } \Omega, \\ \phi &= 0 && \text{on } \Gamma_D, \\ \psi \cdot \nu &= 0 && \text{on } \Gamma_N. \end{aligned}$$

The lowest order Raviart-Thomas [21, 10] finite element discretization on grid G^k gives a saddle point system with our discrete divergence matrix B^k. If $\Gamma_D \neq \emptyset$, there

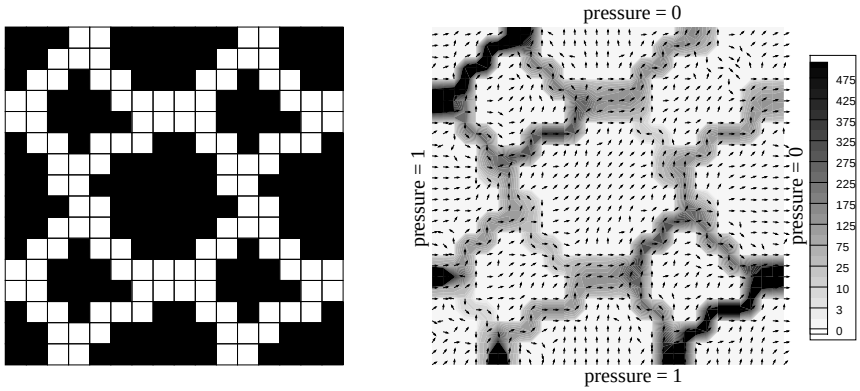

FIG. 4.1. *Left: A Darcy-Stokes system obtained from Fig. 4.3 by removing disconnected vugs. Darcy elements are in black, and Stokes in white. Right: Fluid velocity obtained with our multigrid algorithm. Arrows indicate the direction of the flow, and gray tones indicate speed (darker being greater).*

is a unique solution, so we have a (discrete) function ψ_h such that $(B^k)^t\psi_h = p$. Then $p \cdot p = (B^k)^t\psi_h \cdot p = \psi_h \cdot B^k p = 0$, and $p = 0$ follows. If $\Gamma_D = \emptyset$, the problem is well posed for $p \in V_p^k/\mathbb{R}$, and again in this case we can conclude that $p = 0$. □

4. Numerical tests of the multigrid solver. We illustrate the performance of our multigrid method by computing the flow for a few two dimensional problems. In this section, we use a relatively poor smoother compared to that presented in §3.5. We simply use an unmodified Uzawa smoother and take $C = \mathrm{diag}(B^t\hat{A}^{-1}B)$. This emphasizes the multigrid procedure itself, and allows us to assess its value in solving (1.11) as opposed to the effectiveness of the smoother.

First, we consider the Darcy-Stokes system shown in the left of Fig. 4.1. Boundary conditions are determined by setting $p_D = 1$ on the left and lower edges, and $p_D = 0$ on the other two edges. Obviously, matrix A in (1.11) depends on the spatial arrangement of the Darcy and Stokes subdomains. The more intertwined they are, the more irregular the coefficients of A will be. This example is clearly very intertwined and has a connected vug network.

The right of Fig. 4.1 shows the velocity field that we obtained. The stopping criterion used was that the scaled difference between two consecutive smoothing iterations on the finest grid be smaller than 10^{-12}. Notice the large jumps in the flux per unit length between different regions. The fluxes in the porous matrix and in the disconnected vugs have values between 10^{-7} and 10^{-5}, while the fluxes in the connected vugs are in the range of several hundreds (up to about 400). As mentioned in §3.3, taking into account the very different orders of magnitude of the Darcy and Stokes flows is crucial in order to obtain a convergent multigrid algorithm. In fact, if we run our multigrid code with different values for parameter $\phi(\varepsilon_1, \varepsilon_2)$ (see (3.9) and (3.10)), we observe that non-physical values make the algorithm diverge.

In most cases where a multigrid algorithm is investigated, the continuous differential problem to be solved is independent of the discretization of the domain. For example, we might want to solve Laplace's equation with appropriate boundary conditions. In order to analyze the convergence factor, the method that is being studied is tested for a set of domain discretizations. In our case, things are different because equation (2.1) depends on the spatial arrangement of the Darcy and Stokes subdo-

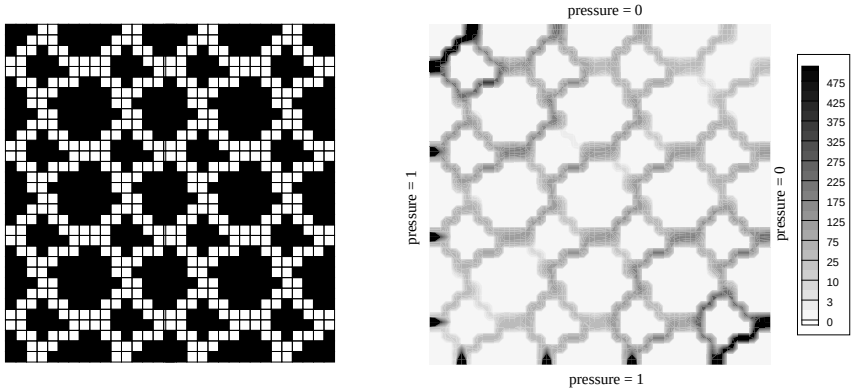

FIG. 4.2. *Left: A Darcy-Stokes system obtained by combining 4 replicas of the system shown in Fig. 4.1 and rescaling. Darcy elements are in black, and Stokes in white. Right: Fluid velocity obtained with our multigrid algorithm. Arrows indicate the direction of the flow, and gray tones indicate speed (darker being greater).*

TABLE 4.1
Measured convergence factors and averaged convergence factors for different discretizations of the system of Figs. 4.1–4.2.

	$h = 1/16$	$h = 1/32$	$h = 1/64$	$h = 1/128$
ρ^n	0.03780	0.04591	0.03908	0.03862
$\tilde{\rho}^n$	0.03901	0.04569	0.03379	0.03662

mains. Therefore, to study the convergence factor, we need to consider decreasingly smaller values of h for the *same type of system*, i.e., one with a similar vug structure. To achieve this effect, we combine 4 replicas of systems with mesh size h like the one shown in Fig. 4.1, and then rescale to obtain a system with mesh size $h/2$, as depicted in Fig. 4.2. We then repeat this process to obtain a family of systems with the same pattern of Darcy-Stokes intertwining and progressively smaller mesh sizes. Obviously, the measured convergence factor will depend on the specific pattern of Darcy-Stokes intertwining.

The measured convergence factor ρ^n and averaged convergence factor $\tilde{\rho}^n$ were computed using the formulas

$$\rho^n = \frac{\|r^n\|}{\|r^{n-1}\|} \quad \text{and} \quad \tilde{\rho}^n = (\rho^2 \rho^3 ... \rho^n)^{1/(n-1)},$$

where r^n is the residual after the nth multigrid iteration and $\|\cdot\|$ denotes the discrete l_2 norm. The results shown in Table 4.1 correspond to the systems of Figs. 4.1 ($h = 1/16$) and 4.2 ($h = 1/32$) and two finer discretizations ($h = 1/64$ and $h = 1/128$). The coarsest grid was 8×8 elements. As the results show, the measured convergence factor of our multigrid method is independent of the size of the system, or equivalently, independent of the mesh size h.

An important feature of the vuggy media considered above is that they have no disconnected vugs. An example of a system with disconnected vugs is shown in Fig. 4.3, which has been obtained from that of Fig. 4.1 by adding six disconnected vugs (i.e., by removing porous matrix material). Note that the solution is almost the same as that of Fig. 4.1.

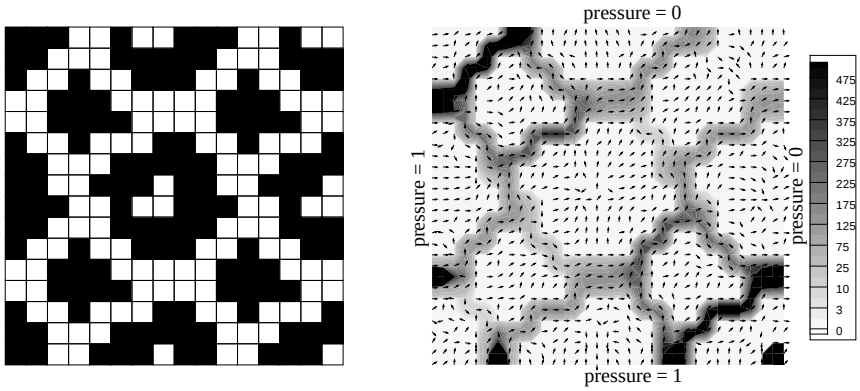

FIG. 4.3. *Left: A domain representing a vuggy porous medium. Darcy elements are in black, and Stokes in white. Right: Fluid velocity obtained with our multigrid algorithm. Arrows indicate the direction of the flow, and gray tones indicate speed (darker being greater).*

The measured convergence factor for this disconnected vug system was only 0.59, and, in general, it was not independent of the mesh size. Moreover, for some systems with disconnected vugs, the convergence rate is very slow unless the coarsest grid is sufficiently fine. This is not surprising, since it is well known that multigrid methods for a system such as (1.11) which have both positive and negative eigenvalues require a coarsest grid large enough in order for some components of the error to be eliminated [9]. In general, the better smoother of §3.5 is needed to solve problems with disconnected vugs.

5. A study of effective permeability properties of vuggy media. In this section, we study the influence of the vug geometry on the macroscale flow properties of the medium. The Darcy-Stokes system described by (1.1)–(1.10) can be considered as a micromodel, since it takes into account all the details about the microscopic geometry of the medium and the interaction between the porous rock and the vugs, and the equations are either based on first principles or strongly supported by experiments. However, this micromodel is computationally expensive.

The macromodel derived in [4] is obtained from the micromodel, appropriately scaled, using homogenization theory under certain mathematical assumptions. The macroscopic model is given by a Darcy equation (i.e., an equation like (1.1) on the entire domain Ω) with a computable effective macroscopic permeability tensor that depends on the vug geometry. Although some of the mathematical assumptions used in this derivation, such as the assumed periodicity of the medium geometry, are not physically accurate, the theory is useful for justifying that the macroscale behavior of the Darcy-Stokes system (1.1)–(1.10) is Darcy-like with an effective permeability.

The effective macroscopic permeability tensor, as given by homogenization theory, was computed in [3] in two dimensional space. It provided an investigation into the influence of the vug geometry on the flow properties of the medium. We perform a similar investigation here in three dimensions, and arrive at a similar conclusion that vug connectivity is the main factor influencing the macroscopic flow properties of a vuggy medium. However, our computational analysis will be somewhat simpler, in that we compute linear flows to approximate the effective permeability, rather than imposing periodic boundary conditions as required in [4].

We estimate only the diagonal elements of the effective permeability tensor. To fix

ideas, suppose we want to estimate the effective permeability in the x-direction, $\bar{K}_{1,1}$, the formula being analogous for the other directions. Using our three dimensional solver, we first compute the flow $\mathbf{u} = (u_1, u_2, u_3)$ in the reference domain that results from applying boundary conditions representing a constant pressure drop δp from left to right in the x-direction, and imposing zero normal flow through the other four faces parallel to the x-direction. We then compute the average flow in the x-direction through the outflow face, f_x, which is

$$u_{1,\text{avg}} = \frac{1}{\text{Area}(f_x)} \int_{f_x} u_1(x, y, z)\, dy\, dz, \tag{5.1}$$

where Area(A) is the area of the face. By mass conservation and the no-flow lateral boundary conditions, $u_{1,\text{avg}}$ could be computed on the inflow face, or even taken as the average of u_1 over the entire domain. Finally, we define $\bar{K}_{1,1}$ from Darcy's law

$$\bar{K}_{1,1} = -\mu u_{1,\text{avg}}/\delta p. \tag{5.2}$$

We present several computational results that show the influence of the vug geometry on the effective permeability in three dimensional space. In each case, we consider a small reference domain with a certain vug configuration. Four cases are studied: a straight vug channel, a constricted vug channel, a meandering vug channel, and disconnected vugs. An x-y cross-section of the four main domains studied are depicted in Fig. 5.1, although we also consider a truly three dimensional meandering vug channel in Fig. 5.2. In all cases, the reference domain Ω is a cubic sample with dimensions 8 cm $\times$ 8 cm $\times$ 8 cm, the porous rock subdomain Ω_d has permeability $K = 10$ md (except where noted), and the Beavers-Joseph coefficient $\alpha = 1$. Generally, the vug channel's cross section is a square of side length $\delta = 1$ cm. Nonzero flow results everywhere in the domain, but it is concentrated in the vug channel.

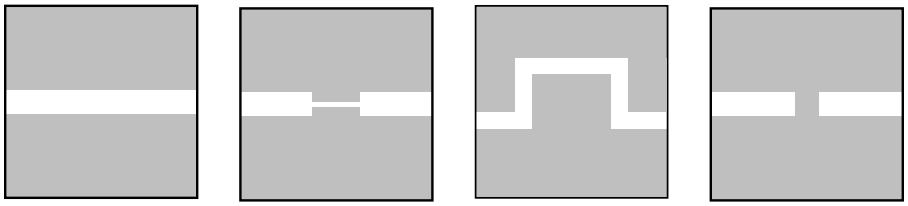

FIG. 5.1. *Cross-section of the four main test domains. The Darcy region is gray, and the Stokes region is white.*

5.1. Straight vug channel. Fig. 5.1A shows a two dimensional cross-section of the three dimensional reference domain containing a horizontal channel. We first examine the effective permeability for different vug apertures. The results are shown in Table 5.1. The index $j = 1$ in $\bar{K}_{j,j}$ corresponds to the horizontal or x-direction, $j = 2$ and $j = 3$ correspond to the y- and z-directions, respectively. We observe that connected Stokes flow paths produce a great increase in the effective permeability. Even a channel with an aperture 2.5 mm gives rise to an effective permeability 5 orders of magnitude greater than the porous rock permeability. The values of $\bar{K}_{2,2}$ and $\bar{K}_{3,3}$ for the effective permeabilities in the y- and z-directions show that a disconnected Stokes flow path has a minor effect on the effective permeability, since the flow is limited by the porous matrix.

TABLE 5.1
Computed effective permeabilities for a straight vug medium ($K = 10$ md).

δ (cm)	$\bar{K}_{1,1}$ (md)	$\bar{K}_{2,2} = \bar{K}_{3,3}$ (md)
1	8.6498e+8	16.879
0.5	5.0856e+7	11.271
0.25	3.4560e+6	10.246

TABLE 5.2
Effect of matrix permeability on the effective permeability of a straight vug medium ($\delta = 1$ cm).

K (md)	$\bar{K}_{1,1}$ (md)	$\bar{K}_{2,2} = \bar{K}_{3,3}$ (md)
1	8.64979e+8	1.6896
10	8.64982e+8	16.879
100	8.64997e+8	168.50
1000	8.65104e+8	1685.1

We next changed the porous rock permeability K, while keeping the same vug aperture $\delta = 1$ cm. As shown in Table 5.2, the effect of the presence of the channel on $\bar{K}_{1,1}$ is much more important than that of a high rock permeability. On the other hand, since the flow in the y- and z-directions is basically determined by the porous matrix, the value of the matrix permeability K has a strong effect on the effective permeabilities $\bar{K}_{2,2}$ and $\bar{K}_{3,3}$.

5.2. Constricted vug channel. The aperture of a vug channel does not remain constant throughout its trajectory. Therefore, we analyze the effect of constricted vugs on the effective permeability. Fig. 5.1B shows a cell with a central vug that is constricted in the middle. The aperture of the vug is 1 cm $\times$ 1 cm. The constricted part is 2 cm long and has cross section 2.5 mm $\times$ 2.5 mm. We obtained $\bar{K}_{1,1} = 7.85507\text{e+}6$ md and $\bar{K}_{2,2} = \bar{K}_{3,3} = 15.1971$ md. If we compare this values with the effective permeabilities for the unconstricted vug configuration ($\bar{K}_{1,1} = 8.64982\text{e+}8$ md, $\bar{K}_{2,2} = \bar{K}_{3,3} = 16.879$ md), we conclude that even very localized constrictions have a major effect on the macroscopic properties of the flow. Moreover, the value of $\bar{K}_{1,1}$ obtained for a 2 cm long constriction is of the same order of magnitude as that obtained for a straight vug medium with channels 2.5 mm $\times$ 2.5 mm ($\bar{K}_{1,1} = 3.4560\text{e+}6$ md, $\bar{K}_{2,2} = \bar{K}_{3,3} = 10.246$ md). This confirms the important effect of constrictions on effective permeability.

5.3. Meandering vug channels. Since natural vug channels tend to change direction, we consider two meandering vug configurations. The first case is analogous to the two dimensional case, since the meandering vug channel stays in the same plane throughout its trajectory. In the second case, the channel does not remain in the same plane.

The first case is illustrated in Fig. 5.1C. If a pressure gradient is applied in the x-direction, the flow through the channel will be in the x- and z-directions. The channel has cross section 1 cm $\times$ 1 cm. The effective permeabilities are $\bar{K}_{1,1} = 2.46928\text{e+}7$ md, $\bar{K}_{2,2} = 16.967$ md, and $\bar{K}_{3,3} = 19.3631$ md. We notice that $\bar{K}_{1,1}$ is smaller and $\bar{K}_{3,3}$ is larger than those values obtained for the straight vug case ($\bar{K}_{1,1} = 8.64982\text{e+}8$ md, $\bar{K}_{2,2} = \bar{K}_{3,3} = 16.879$ md), as should be expected.

The second meandering configuration is shown in Fig. 5.2. Actually, the figure

TABLE 5.3
Effect of vug disconnection by varying plug size on effective permeability.

plug length (cm)	$\bar{K}_{1,1}$ (md)	$\bar{K}_{2,2} = \bar{K}_{3,3}$ (md)
1	38.54	16.92
0.5	50.63	17.01
0.25	88.69	17.27

depicts the flow velocity, which clearly shows both the location of the vug channel and the fact that the flow is nonzero in the matrix rock. If a pressure gradient is applied in the x-direction, the flow through the channel will be in the three spatial directions. We obtain $\bar{K}_{1,1} = 1.64619\text{e+}6\,\text{md}$, $\bar{K}_{2,2} = 18.465\,\text{md}$, and $\bar{K}_{3,3} = 18.589\,\text{md}$. The value for $\bar{K}_{1,1}$ is lower than that for the previous meandering configuration and of the same order of magnitude as that obtained for the constricted vug ($\bar{K}_{1,1} = 7.85507\text{e+}6\,\text{md}$, $\bar{K}_{2,2} = \bar{K}_{3,3} = 15.1971\,\text{md}$). Note also the increase in the effective permeabilities in the y- and z-directions compared to the straight vug medium. These results show that in three dimensions, the effect of meandering channels is more complex than in the two dimensional case. Also, three dimensional meandering vugs and constricted vugs may have similar effects on the flow properties of vuggy media.

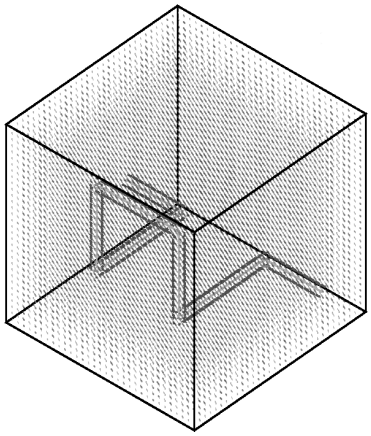

FIG. 5.2. *A meandering vug channel in three dimensional space. Depicted is the flow velocity, which clearly shows the location of the vug channel.*

5.4. Disconnected vugs. Flow experiments suggest that the degree of vug connectivity varies throughout a vuggy porous medium and that it has a major effect on the flow properties of the rock [29]. Lastly we consider a configuration where the flow through a channel is completely interrupted by a small plug of porous rock. This is depicted in Fig. 5.1D. The vug aperture is $1\,\text{cm} \times 1\,\text{cm}$ and the plug length varies from 2.5 mm to 1 cm. The effective permeabilities are shown in Table 5.3. We notice that even if the length of the plug is 2.5 mm, the effective permeability is quite similar to that of the porous rock. We had seen that a vug with a very small constriction produces an effective permeability of about 1e+6 md, indicating that connected and disconnected vugs give rise to very different macroscopic flow properties. We conclude that the degree of connectivity of the vugs is the most important factor influencing the macroscopic flow properties of the medium.

Overall, our three dimensional numerical studies have confirmed that the presence of vugs, their orientation and shape, and most importantly, their interconnectivity, determine the effective permeability and, therefore, the macroscopic flow properties of the medium.

REFERENCES

[1] R. E. Alcouffe, A. Brandt, J. E. Dendy, and J. W. Painter, *The multi-grid method for the diffusion equation with strongly discontinuous coefficients*, SISC, 2 (1981), pp. 430–454.

[2] T. Arbogast and D. S. Brunson, *A computational method for approximating a Darcy-Stokes system governing a vuggy porous medium*, Comput. Geosci., 11 (2007), pp. 207–218.

[3] T. Arbogast, D. S. Brunson, S. L. Bryant, and J. W. Jennings, *A preliminary computational investigation of a macro-model for vuggy porous media*, in Computational Methods in Water Resources XV, C. T. Miller et al., eds., New York, 2004, Elsevier.

[4] T. Arbogast and H. L. Lehr, *Homogenization of a Darcy-Stokes system modeling vuggy porous media*, Comput. Geosci., 10 (2006), pp. 291–302.

[5] T. Arbogast and M. F. Wheeler, *A family of rectangular mixed elements with a continuous flux for second order elliptic problems*, SIAM J. Numer. Anal., 42 (2005), pp. 1914–1931.

[6] G. S. Beavers and D. D. Joseph, *Boundary conditions at a naturally permeable wall*, J. Fluid Mech., 30 (1967), pp. 197–207.

[7] J. H. Bramble and J. E. Pasciak, *A preconditioning technique for indefinite systems resulting from mixed approximations of elliptic problems*, Math. Comp., 50 (1988), pp. 1–17.

[8] J. H. Bramble, J. E. Pasciak, and A. T. Vassilev, *Analysis of the inexact Uzawa algorithm for saddle point problems*, SIAM J. Numer. Anal., 34 (1997), pp. 1072–1092.

[9] A. Brandt, *Multi-level adaptive solutions to boundary-value problems*, Math. Comp., 31 (1977), pp. 333–390.

[10] F. Brezzi and M. Fortin, *Mixed and hybrid finite element methods*, Springer-Verlag, New York, 1991.

[11] D. S. Brunson, *Simulating fluid flow in vuggy porous media*, PhD thesis, Department of Mathematics, The University of Texas at Austin, Austin, Texas, August 2005.

[12] E. Burman and P. Hansbo, *A unified stabilized method for Stokes' and Darcy's equations*, J. Comput. Appl. Math., 198 (2007), pp. 35–51.

[13] M. Discacciati, *Domain decomposition methods for the coupling of surface and groundwater flows*, PhD thesis, Ecole Polytechnique Fédérale de Lausanne, 2004.

[14] M. Discacciati, E. Miglio, and A. Quarteroni, *Mathematical and numerical models for coupling surface and groundwater flows*, Appl. Numer. Math., 43 (2002), pp. 57–74.

[15] M. Fortin, *Old and new finite elements for incompressible flows*, Int. J. Numer. Meth. Fluids, 1 (1981), pp. 347–364.

[16] J. Galvis and M. Sarkis, *Non-matching mortar discretization analysis for the coupling Stokes-Darcy equations*, Electron. Trans. Numer. Anal., 26 (2007), pp. 350–384.

[17] D. K. Gartling, C. E. Hickox, and R. C. Givler, *Simulation of coupled viscous and porous flow problems*, Comp. Fluid Dyn., 7 (1996), pp. 23–48.

[18] W. Hackbusch and U. Trottenberg, eds., *Multigrid methods II: proceedings of the 2nd European Conference on Multigrid Methods, held at Koln, October 1-4, 1985*, Lecture notes in mathematics 1228, Springer-Verlag, Berlin, 1986.

[19] I. P. Jones, *Low Reynolds number flow past a porous spherical shell*, Proc. Camb. Phil. Soc., 73 (1973), pp. 231–238.

[20] W. J. Layton, F. Schieweck, and I. Yotov, *Coupling fluid flow with porous media flow*, SIAM. J. Numer. Anal., 40 (2003), pp. 2195–2218.

[21] R. A. Raviart and J. M. Thomas, *A mixed finite element method for 2nd order elliptic problems*, in Mathematical Aspects of Finite Element Methods, I. Galligani and E. Magenes, eds., no. 606 in Lecture Notes in Math., Springer-Verlag, New York, 1977, pp. 292–315.

[22] B. Rivière and I. Yotov, *Locally conservative coupling of Stokes and darcy flows*, SIAM. J. Numer. Anal., 42 (2005), pp. 1959–1977.

[23] J. E. Roberts and J.-M. Thomas, *Mixed and hybrid methods*, in Handbook of Numerical Analysis, P. G. Ciarlet and J. L. Lions, eds., vol. 2, Elsevier Science Publishers B.V. (North-Holland), Amsterdam, 1991, ch. Finite Element Methods (Part 1), pp. 523–639.

[24] J. Ruge and K. Stüben, *Algebraic multigrid (amg).*, in Multigrid methods, S. F. McCormick, ed., Frontiers in Applied Mathematics, SIAM, Philadelphia, 1987, pp. 73–130.

[25] P. G. Saffman, *On the boundary condition at the interface of a porous medium*, Studies in

Applied Mathematics, 1 (1971), pp. 93–101.
[26] A. G. Salinger, R. Aris, and J. J. Derby, *Finite element formulations for large-scale, coupled flows in adjacent porous and open fluid domains*, International Journal for Numerical Methods in Fluids, 18 (1994), pp. 1185–1209.
[27] K. Stüben, *A review of algebraic multigrid. Numerical Analysis 2000, vol VII, Partial Differential Equations*, J. Comput. Appl. Math., 128 (2001), pp. 281–309.
[28] U. Trottenberg, C. Oosterlee, and A. Schüller, *Multigrid*, Academic Press, 2001.
[29] L. Zhang, *Multiscale flow and transport in highly heterogeneous carbonates*, PhD thesis, Department of Petroleum and Geosystems Engineering, The University of Texas at Austin, Austin, Texas, August 2005.